

**Cs<sub>2</sub>AgBiBr<sub>6-x</sub>Cl<sub>x</sub> solid solutions – Band gap engineering  
with halide double perovskites**

Journal:	<i>Journal of Materials Chemistry C</i>
Manuscript ID	TC-ART-05-2019-002674.R1
Article Type:	Paper
Date Submitted by the Author:	25-Jun-2019
Complete List of Authors:	Gray, Matthew; Ohio State University, Department of Chemistry and Biochemistry McClure, Eric; Ohio State University, Department of Chemistry and Biochemistry Woodward, Patrick; Ohio State University, Department of Chemistry and Biochemistry



## ARTICLE

## Cs<sub>2</sub>AgBiBr<sub>6-x</sub>Cl<sub>x</sub> solid solutions – Band gap engineering with halide double perovskites

Matthew B. Gray<sup>a</sup>, Eric T. McClure<sup>a</sup>, and Patrick M. Woodward<sup>a,\*</sup>

Received 00th January 20xx,  
Accepted 00th January 20xx

DOI: 10.1039/x0xx00000x

www.rsc.org/

The halide double perovskites Cs<sub>2</sub>AgBiBr<sub>6</sub> and Cs<sub>2</sub>AgBiCl<sub>6</sub> form a complete solid solution. The cubic *Fm*<sup>3</sup>*m* space group symmetry and near complete rock salt ordering of Ag<sup>+</sup> and Bi<sup>3+</sup> are retained for all compositions, and the lattice parameter varies linearly between the two end-members. The band gap increases linearly between Cs<sub>2</sub>AgBiBr<sub>6</sub> (*E<sub>g</sub>* = 2.19 eV) and Cs<sub>2</sub>AgBiBrCl<sub>5</sub> (*E<sub>g</sub>* = 2.61 eV), but deviates upward from a Vegard's Law behavior once the chloride content exceeds ~85%. The Cs<sub>2</sub>AgBiCl<sub>6</sub> end-member has a band gap, *E<sub>g</sub>* = 2.77 eV, that is 0.10 eV larger than the extrapolated value from a Vegard's Law fit. Analysis of the powder X-ray diffraction peak shapes shows that microstrain increases steadily as the Cl<sup>-</sup> content increases, before dropping precipitously for the Cs<sub>2</sub>AgBiCl<sub>6</sub> end-member. The combined results give no evidence for long range ordering of halide ions.

### Introduction

Halide perovskites with the general formula ABX<sub>3</sub> (A = Cs<sup>+</sup>, CH<sub>3</sub>NH<sub>3</sub><sup>+</sup>; B = Pb<sup>2+</sup>, Sn<sup>2+</sup>, Ge<sup>2+</sup>; X = I<sup>-</sup>, Br<sup>-</sup>, Cl<sup>-</sup>) have been widely studied for use in a variety of optoelectronic applications, most notably as the absorbing layer in photovoltaic cells.<sup>1-5</sup> Inorganic halide double perovskites with formula A<sub>2</sub>B<sup>I</sup>B<sup>III</sup>X<sub>6</sub> (A = Cs<sup>+</sup>, Rb<sup>+</sup>; B<sup>I</sup> = Ag<sup>+</sup>, K<sup>+</sup>, Na<sup>+</sup>, Li<sup>+</sup>; B<sup>III</sup> = Bi<sup>3+</sup>, Sb<sup>3+</sup>, In<sup>3+</sup>; X = I<sup>-</sup>, Br<sup>-</sup>, Cl<sup>-</sup>) are site-ordered variants of the perovskite structure that exhibit an alternating (rock salt) pattern of B<sup>I</sup> and B<sup>III</sup> ions on the octahedral sites. Double perovskites are attractive because they do not contain the toxic Pb<sup>2+</sup> ion and offer enhanced chemical and thermal stability, particularly with respect to the tin and germanium halide perovskites. While many A<sub>2</sub>B<sup>I</sup>B<sup>III</sup>Cl<sub>6</sub> double perovskites can be prepared, very few examples of bromide and iodide analogues have been reported, Cs<sub>2</sub>AgBiBr<sub>6</sub> being the most notable exception.<sup>6</sup> The lack of iodide double perovskites, which hold the promise for sub 2 eV band gaps, has limited their use in solar cells. Nevertheless, a photovoltaic cell with a power conversion efficiency of 2.5% has been reported for Cs<sub>2</sub>AgBiBr<sub>6</sub>.<sup>7</sup> The wider band gaps of double perovskites appear to be more suitable for tandem solar cells. For that application, and others, the ability to tune the band gap of the absorbing layers is essential to match energy levels of the device components.<sup>8</sup> In this work, we report on a facile method to tune the band gap of the double perovskite solid solution, Cs<sub>2</sub>AgBiBr<sub>6-x</sub>Cl<sub>x</sub>, by halide substitution.

### Experimental

With the exception of AgCl, all reagents were commercially purchased and used without modification. Reagents included HCl (Fisher Scientific, 37%), HBr (Sigma Aldrich, 47%), HI (Sigma

Aldrich, 47+%), H<sub>3</sub>PO<sub>2</sub> (Sigma Aldrich, 50%), Bi<sub>2</sub>O<sub>3</sub> (J.T. Baker, 99%), BiI<sub>3</sub> (Sigma Aldrich, 99%), AgBr (Alfa Aesar, 99.5%), AgI (Alfa Aesar, 99.9%), CsCl (Alfa Aesar, 99.9%), CsBr (Alfa Aesar, 99%), CsI (Alfa Aesar, 99.9%), PbCl<sub>2</sub> (Alfa Aesar, 99%), and PbBr<sub>2</sub> (Alfa Aesar, 98+%). AgCl was synthesized on a gram scale via a precipitation reaction between KCl (Fisher Scientific, 99.8%) and AgNO<sub>3</sub> (Alfa Aesar, 99.9%). The resulting white product was washed three times with deionized H<sub>2</sub>O and dried overnight via vacuum filtration; the filter flask was covered with aluminum foil to prevent photoreduction of Ag(I) into Ag(0).

The double perovskites, Cs<sub>2</sub>AgBiBr<sub>6</sub> and Cs<sub>2</sub>AgBiCl<sub>6</sub>, were synthesized following a modified procedure from the literature.<sup>6</sup> For a 2.00 gram synthesis, 18.0 mL of concentrated HCl and 2.0 mL of H<sub>3</sub>PO<sub>2</sub> (18.0 mL of concentrated HBr and 2.0 mL of H<sub>3</sub>PO<sub>2</sub>) were heated to 120 °C. To this solution, 1.26 mmol of Bi<sub>2</sub>O<sub>3</sub> (0.942 mmol of Bi<sub>2</sub>O<sub>3</sub>) and 2.51 mmol of AgCl (1.88 mmol of AgBr) were added. The acid was stirred for 15 minutes to allow the reagents to dissolve, forming a homogeneous solution. 5.03 mmol of CsCl (3.77 mmol of CsBr) was then added, immediately triggering the precipitation of the desired perovskite with near unity yield. The final product mass to initial solution volume ratio was kept at 1.00 g of perovskite to 10.0 mL of acid solution throughout all experiments. The resulting precipitate was collected on filter paper, washed with neat ethanol three times, and dried overnight via vacuum filtration.

The solid solutions, Cs<sub>2</sub>AgBiBr<sub>6-x</sub>Cl<sub>x</sub> [nominally x = 1, 2, 3, 4, 4.5, 5, 5.5], were prepared via the solid-state synthesis from the end-members. Appropriate molar ratios (5:1, 4:2, 3:3, 2:4, 1.5:4.5, 1:5, and 0.5:5.5) of the double perovskite end-members were ground for 20 minutes with an agate mortar and pestle in an argon-filled glove box. The samples were then placed in covered alumina crucibles and heated in a box furnace in air at 200 °C for 18 hours. One cycle of heating was sufficient to produce homogeneous solid solutions.

Purity of all compounds was confirmed using powder X-ray diffraction (PXRD); no secondary phases were detected. Synthesis of the solid solutions annealed at 200 °C for 18 hours produced powders that were easily ground, with colors ranging from hunter orange to pale yellow, depending on the ratio of the starting materials.

<sup>a</sup> Department of Chemistry and Biochemistry, The Ohio State University, 100 W. 18th Avenue, Columbus, Ohio 43210, United States

\*Corresponding Author: woodward.55@osu.edu

#### ORCID

Matthew B. Gray: 0000-0002-9526-4732

Eric T. McClure: 0000-0003-1432-0016

Patrick M. Woodward: 0000-0002-3441-2148

Electronic Supplementary Information (ESI) available: [details of any supplementary information available should be included here]. See DOI: 10.1039/x0xx00000x

Solid state synthesis of an iodide containing double perovskite phase,  $\text{Cs}_2\text{AgBiBr}_{6-x}\text{I}_x$ , was attempted at a variety of halide ratios ( $x = 3, 2, 1, 0.33$ ). Direct synthesis from binary starting materials yielded a mixture of undesired products ( $\text{AgX}$  and  $\text{Cs}_3\text{Bi}_2\text{X}_9$  [ $X = \text{Br}, \text{I}$ ]) without the appearance of a perovskite phase, while syntheses from the  $\text{Cs}_2\text{AgBiBr}_6$  double perovskite and appropriate binary iodide reagents yielded a slight increase in the perovskite lattice constant with respect to  $\text{Cs}_2\text{AgBiBr}_6$ , but significant amounts of the  $\text{Cs}_3\text{Bi}_2\text{I}_9$  and  $\text{AgBr}$  phases were always present in the PXRD patterns. Attempts to determine the iodide solubility in  $\text{Cs}_2\text{AgBiBr}_{6-x}\text{I}_x$  and/or the shift in band gap were frustrated by the presence of  $\text{Cs}_3\text{Bi}_2\text{I}_9$  ( $E_g = 2.1$  eV) whose diffraction peaks overlap significantly with the double perovskite phase. It would appear as though there is little to no iodide solubility in the bromide end-member.

Powder X-ray diffraction (PXRD) data were collected on a Bruker D8 Advance powder diffractometer (40 kV, 40 mA, sealed Cu X-ray tube) equipped with an incident beam monochromator (Johansson type  $\text{SiO}_2$ -crystal) and a Lynxeye XE-T position sensitive detector. Rietveld refinements of laboratory PXRD data were carried out using the TOPAS-Academic (Version 6) software package to determine the crystal structure.<sup>9</sup> A Rigaku MiniFlex II benchtop powder X-ray diffractometer (30 kV, 15 mA, sealed Cu X-ray tube, with a NaI scintillation detector) was used for initial phase identification. Search/Match routines were performed using the Materials Data, Inc., software Jade.<sup>10</sup>

UV-visible diffuse reflectance data were collected from 178 nm to 890 nm with an Ocean Optics USB4000 spectrometer equipped with a Toshiba TCD1304AP (3648-element linear silicon CCD array). The spectrometer was used with an Ocean Optics DH-2000-BAL deuterium and halogen UV-vis-NIR light source and a 400  $\mu\text{m}$  R400-7-ANGLE-VIS reflectance probe. The detector was calibrated using a Spectralon diffuse reflectance standard.

## Results

The PXRD patterns of the  $\text{Cs}_2\text{AgBiBr}_{6-x}\text{Cl}_x$  samples across the entire series are shown in Fig. 1. All solid solution members adopt the cubic double perovskite structure with  $Fm\bar{3}m$  space group symmetry. A representative example of a Rietveld refinement of the  $\text{Cs}_2\text{AgBiBr}_3\text{Cl}_3$  composition is shown in Fig. S1.

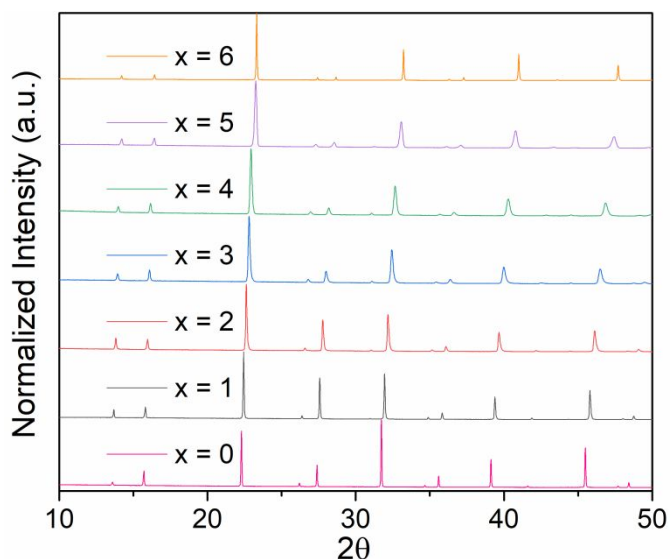


**Fig. 1** Powder X-ray diffraction patterns for the solid solution series  $\text{Cs}_2\text{AgBiBr}_{6-x}\text{Cl}_x$ .

The refined cubic lattice parameters of the solid solution members were examined as a function of the nominal anion composition. A linear increase of the lattice occurred as the bromide ion content increased, in accordance with Vegard's Law, as shown in Fig. 2, indicating the anion contents were close to the nominal values expected from the starting ratios of the two end members. When the anion site occupancy was refined in the Rietveld analysis of the XRPD data, chloride occupancies within a few percent of the nominal values were obtained (Table S2).

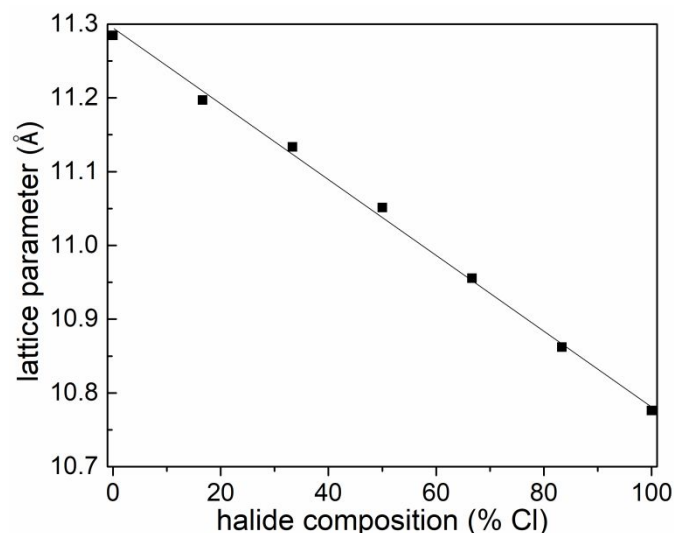


**Fig. 2** Cubic lattice parameters for  $\text{Cs}_2\text{AgBiBr}_{6-x}\text{Cl}_x$  samples as a function of the chloride content. Error bars for the lattice parameter are smaller than the symbols.

Notice in Fig. 1 that the Bragg peaks in the PXRD patterns are broader for the samples with a mixture of halide ions than they are for the end-members. To determine if this is due to microstrain or crystallite size effects, the peak broadening was analyzed using TOPAS-Academic (Version 6).<sup>9</sup> Instrumental broadening was estimated from the PXRD spectrum of the  $\text{Cs}_2\text{AgBiBr}_6$  end-member, whose peak widths were comparable to calibration standards, indicating minimal size or strain broadening. For the remaining samples the peak shape and axial divergence parameters were fixed at the values obtained from the  $\text{Cs}_2\text{AgBiBr}_6$  refinement, and the additional broadening was modelled using the microstrain and crystallite size macros. Using this approach, it was determined that nearly all the sample broadening could be attributed to microstrain broadening, primarily Gaussian in nature, so the refinements were carried out with no crystallite size broadening. Full details are given in the Supporting Information. A substantial improvement in the fit is seen when microstrain broadening is included, as shown in Table S1.

The microstrain values as a function of chloride ion content are plotted in Fig. 3. The strain rises in a near linear fashion as the  $\text{Cl}^-$  content increases before dropping precipitously for  $\text{Cs}_2\text{AgBiCl}_6$ . Microstrain is a measure of the variation in unit cell dimensions throughout the sample. Alloys tend to have a higher microstrain than pure compounds because of the random distribution of atoms/ions of different sizes, which makes it easy

to rationalize why the end-members have much less strain than the solid solutions. It's more difficult to understand why chloride-rich samples have more microstrain than bromide-rich samples. Perhaps squeezing a larger anion ( $\text{Br}^-$ ) into a lattice made up mostly of smaller anions ( $\text{Cl}^-$ ) disrupts the crystal packing to a greater extent than the reverse scenario.

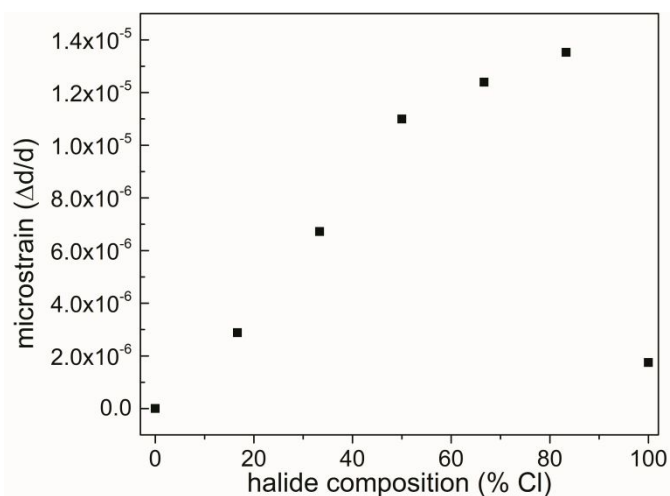


**Fig. 3** Microstrain broadening within the  $\text{Cs}_2\text{AgBiBr}_{6-x}\text{Cl}_x$  solid solution series as a function of the chloride content. Error bars for the microstrain are smaller than the symbols.

To determine its optical band gap a UV-vis diffuse reflectance spectrum (DRS) was collected for each sample prepared (Fig. S2). The end-member compounds exhibit indirect band gaps, as determined by previous experimental and computational analyses.<sup>6,11-13</sup> The absorption onsets seen in the intermediate members of the solid solution had similar slopes to the end-members, and therefore, were assumed to be indirect band gap materials as well.

To extract optical band gaps, the DRS spectra were transformed to pseudoabsorption spectra via the Kubelka-Munk (KM) equation:

$$\alpha = \frac{(1-R)^2}{2R},$$

where  $\alpha$  is the optical absorption coefficient and  $R$  is the reflectance. This equation allows the absorbance of a material to be estimated from its reflectance. The KM plots for the solid solution series are shown in Fig. 4. The Tauc method was applied to the transformed data to estimate the band gaps of these samples. For an indirect band gap semiconductor, the equation  $[F(R)h\nu]^{1/2}$  is used to extract band gaps. The band gap values obtained in this manner are given in Table S3 and plotted as a function of composition in Fig. 5. The asymmetric absorbance peak that lies 0.6–0.7 eV above the band gap is thought to arise due to localized  $\text{Bi } 6s^2 \rightarrow 6s^1 6p^1$  transitions.<sup>14</sup>

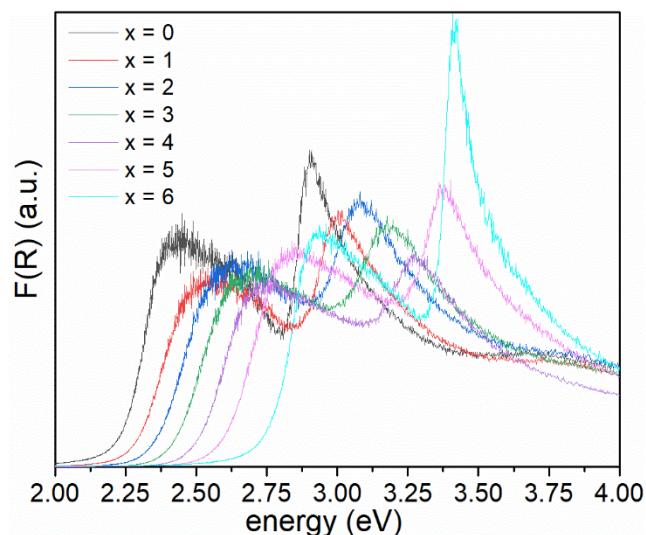


**Fig. 4** Kubelka-Munk transformation of the diffuse reflectance spectroscopy data for the solid solution series  $\text{Cs}_2\text{AgBiBr}_{6-x}\text{Cl}_x$ .

Tuning the band gap by forming solid solutions, so-called band gap engineering, is a powerful tool for optimizing the absolute band positions of semiconductors for use various optoelectronic devices, including tandem solar cells. As shown in Fig. 5 the band gap of  $\text{Cs}_2\text{AgBiBr}_{6-x}\text{Cl}_x$  perovskites increases linearly with increasing  $\text{Cl}^-$  content until  $x \approx 5$ . The band gap of the  $\text{Cs}_2\text{AgBiCl}_6$  end-member is larger by 0.10 eV than predicted from extrapolation of the linear fit to the samples between  $x = 0$  and  $x = 5$ . This is contrary to the trends seen in the  $\text{CH}_3\text{NH}_3\text{PbBr}_{3-x}\text{Cl}_x$  and  $\text{CH}_3\text{NH}_3\text{PbI}_{3-x}\text{Br}_x$  series, where the band gap follows Vegard's Law across the entire solid solution.<sup>15</sup> The energy of the localized  $\text{Bi } 6s^2 \rightarrow 6s^1 6p^1$  transition also shifts to higher energy as the  $\text{Cl}^-$  content increases, by a similar amount as the band gap (see Fig. S3). It is consistently 0.6–0.8 eV higher in energy than the band gap. Unlike the band gap the increase in the energy of this transition is nearly linear across the entire series.

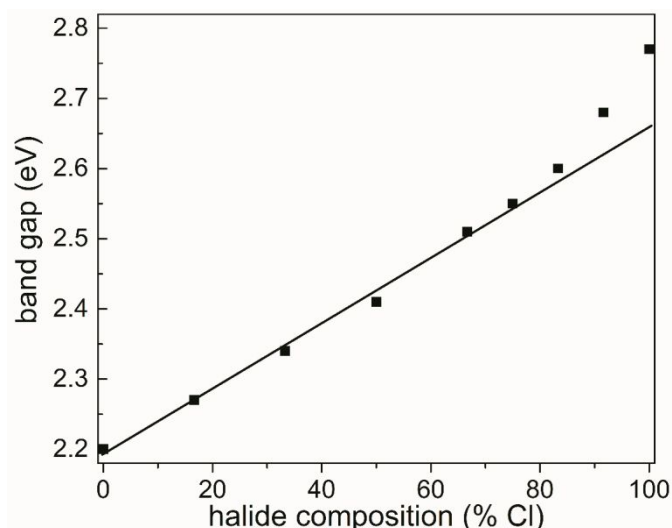


**Fig. 5** Band gap obtained from the KM transformation of the DRS data as a function of chlorine composition in the solid solution series. Error bars for the band gaps are smaller than the symbols.

Band structure calculations on these materials show that the valence to conduction band transition can be described as a transition from filled halogen nonbonding p-orbitals to empty antibonding orbitals with significant bismuth 6p character.<sup>6,11</sup> Not surprisingly, as the content of the more electronegative chloride ion increases the valence band energy is lowered and the band gap increases (Table S3). The reasons behind the deviation of the chloride end-member from Vegard's Law are hard to identify with certainty. However, it is worth noting that the deviation from Vegard's Law occurs when the Cl<sup>-</sup> ion content exceeds 80-85%, close to the composition where it becomes statistically impossible to include at least one bromide ion in every BiX<sub>6</sub> octahedron.

## Conclusions

The halide double perovskites Cs<sub>2</sub>AgBiCl<sub>6</sub> and Cs<sub>2</sub>AgBiBr<sub>6</sub> form a complete solid solution. Attempts to prepare Cs<sub>2</sub>AgBiBr<sub>6-x</sub>Cl<sub>x</sub> were unsuccessful. The Cs<sub>2</sub>AgBiBr<sub>6-x</sub>Cl<sub>x</sub> lattice parameter follows Vegard's Law across the entire solid solution, while the band gap does so from Cs<sub>2</sub>AgBiBr<sub>6</sub> to approximately Cs<sub>2</sub>AgBiBrCl<sub>5</sub>. The band gap deviates upward from a linear Vegard's Law fit for the most chloride-rich compositions. No signs of anion ordering are seen for any composition in the solid solution. The ability to tune the band gaps and absolute band positions of these systems facilitates integration of halide double perovskites into optoelectronic devices.

## Conflicts of interest

There are no conflicts to declare.

## Acknowledgements

Funding for this research was provided by the National Science Foundation under award number DMR-1610631. Special thanks to Nick Harvey and Kelsey Hodge for assistance in starting material preparation.

## Notes and references

- 1 S. Turren-Cruz, A. Hagfeldt, M. Saliba, *Science*, 2018, **362**, 449.
- 2 M.A. Green, Y. Hishikawa, E.D. Dunlop, D.H. Levi, J. Hohl-Ebinger, A.W.Y. Ho-Baillie, *Prog. Photovoltaics Res. Appl.* 2018, **26**, 427.
- 3 J. Werner, C.H. Weng, A. Walter, L. Fesquet, J.P. Seif, S. De Wolf, B. Niesen, C. Ballif, *J. Phys. Chem. Lett.* 2016, **7**, 161.
- 4 H.S. Kim, C.R. Lee, J.H. Im, K.B. Lee, T. Moehl, A. Marchioro, S.J. Moon, R. Humphry-Baker, J.H. Yum, J.E. Moser, M. Gratzel, G. N. Park, *Sci. Rep.* 2012, **2**, 1.
- 5 A. Kojima, K. Teshima Y. Shirai, T. Miyasaka, *J. Amer. Chem. Soc.*, 2009, **131**, 6050.
- 6 E.T. McClure, M.R. Ball, W. Windl, P.M. Woodward, *Chem. Mater.*, 2016, **28**, 1348.
- 7 E. Gruel, M. Petrus, A. Binek, P. Docampo, T. Bein, *J. Mat. Chem. A*, 2017, **5**, 19972.
- 8 J.W. Lee, Y.T. Hsieh, N. De Marco, S.H. Bae, Q. Han, Y. Yang, *J. Phys. Chem. Lett.*, 2017, **8**, 1999.
- 9 *Topas-Academic (Version 6), General Profile and Structural Analysis for Powder Diffraction Data*; Bruker AXS: Karlsruhe, Germany, 2004.
- 10 Materials Data, Inc., Jade 2010.
- 11 A.H. Slavney, T. Hu, A.M. Lindenberg, H.I. Karunadasa, *JACS*, 2016, **138**, 2138.
- 12 A.H. Slavney, L. Leppert, D. Bartesaghi, A. Gold-Parker, M.F. Toney, T.J. Savenije, J.B. Neaton, H.I. Karunadasa, *J. Amer. Chem. Soc.*, 2017, **139**, 5015.
- 13 G. Volonakis, A.A. Haghighirad, R.L. Milot, W.H. Sio, M.R. Filip, B. Wenger, M.B. Johnston, L.M. Herz, H.J. Snaith, F. Giustino, *J. Phys. Chem. Lett.*, 2017, **8**, 772.
- 14 J.D. Majher, M.B. Gray, T.A. Strom, P.M. Woodward, *Chem. Mater.*, 2019, **31**, 1738.
- 15 W. Wang, J Su, L. Zhang, Y. Lei, D. Wang, D. Lu, Y. Bai, *CrystEngComm.*, 2018, **20**, 1635.

The halide double perovskite solid solution  $\text{Cs}_2\text{AgBiBr}_{6-x}\text{Cl}_x$  has been investigated and found to exhibit a band gap that increases from 2.2 eV to 2.8 eV as the  $\text{Cl}^-$  content increases, with an upward deviation from Vegard's law when  $x > 5$ .

